

7A52 铝合金单双丝焊工艺对比分析

张传臣<sup>1</sup>, 陈芙蓉<sup>1</sup>, 高云喜<sup>2</sup>  
(1. 内蒙古工业大学 材料科学与工程学院, 呼和浩特 010051;  
2. 包头北方工程技术开发有限责任公司, 内蒙古 包头 014033)



张传臣

**摘 要:** 采用 ER5356 焊丝对 7A52 铝合金厚板进行单、双丝气体保护焊工艺对比。对单双丝焊焊接接头的变形、显微组织、焊缝硬度和拉伸性能进行了试验分析。结果表明, 双丝焊焊接接头变形小; 双丝焊焊缝与单丝焊焊缝相比, 组织更为细小致密, 热影响区较窄; 焊缝区硬度高于单丝焊焊缝; 焊缝抗拉强度比单丝焊焊缝提高了 7.7%。由能谱分析得知采用双丝焊工艺可抑制锌的挥发。  
**关键词:** 7A52 铝合金; 单丝焊; 双丝焊; 显微组织; 力学性能  
**中图分类号:** TG407      **文献标识码:** A      **文章编号:** 0253—360X(2008)09—0067—04

0 序 言

超硬铝合金 7A52 是近年来新研制的高强可焊铝合金, 该合金经轧制后性能优良。该合金焊接时热裂纹倾向大, 气孔严重, 焊缝强度低, 这些问题一直困扰着国内焊接界, 对于厚板的焊接 (20 ~ 60 mm), 该类问题更加突出, 已经成为制约该合金使用的一个瓶颈。目前对于该合金厚板的焊接, 主要采用单丝熔化极氩弧焊 (MIG), 通常用细焊丝高电流密度来焊接。对于前者而言, 大电流焊接会因焊接热输入过大而导致晶粒严重粗化, 使接头性能降低, 且焊缝成形差、容易产生“皱皮”现象; 后者用细丝大电流密度焊接时, 对送丝速度要求极高, 当送丝速度满足不了时, 焊接则不能正常进行<sup>[1-4]</sup>。

文中通过单双丝 MIG 焊工艺对比, 对 40 mm 7A52 装甲铝合金板材进行施焊, 通过对焊焊接接头组织和硬度以及拉伸性能的对比, 比较单双丝 MIG 焊接工艺对 7A52 铝合金组织和性能的影响, 找出双丝焊在焊接超硬铝合金方面的独特优势, 为双丝焊在铝合金焊接方面的应用提供有价值的试验依据。

1 试验方法

试验材料选用 40 mm 的 Al-Zn-Mg 系 7A52 铝合金板材, 其主要化学成分见表 1, 采用 ER5356 焊丝, 焊丝规格为  $\phi 1.6$  mm, 主要化学成分见表 2, 母材 7A52 的力学性能见表 3。试验所用保护气体为纯氩, 纯度  $\geq 99.99\%$ 。

表 1 7A52 铝合金的主要化学成分(质量分数, %)  
Table 1 Chemical composition of 7A52 alloy

牌号	Zn	Mg	Cu	Mn	Cr	Ti	Zr	Fe	Si	Al
7A52	4.0~4.8	2.0~2.8	0.05~0.20	0.20~0.50	0.15~0.25	0.05~0.18	0.05~0.15	≤0.30	≤0.25	余量

表 2 ER5356 焊丝的化学成分(质量分数, %)  
Table 2 Welding wire composition of ER5356

Cu	Mn	Mg	Cr	Zn	Ti	Al
0.1	0.05~0.20	4.5~5.5	0.05~0.20	0.10	0.06~0.20	余量

双丝焊系统采用两台奥地利 Fronius 公司生产的 TPS5000 多功能数字化焊机、两台送丝机、一把焊

枪及与其配套的 IGM 焊接机器人等进行施焊。单丝焊焊接设备采用 SAF 公司的 TRS—480 半自动脉冲焊机进行施焊。

表 3 7A52 铝合金的力学性能  
Table 3 Mechanical properties of 7A52 alloy

抗拉强度 $R_m$ /MPa	屈服强度 $R_d$ /MPa	断后伸长率 $A(\%)$
≥410	≥345	≥7

其中双丝焊机的两个送丝机采用推拉式送丝, 并通过两根送丝管分别将两根焊丝同时送入焊枪中两个独立的导电嘴, 确保焊接过程送丝通畅, 且焊丝在双电弧中被熔化, 形成一个熔池, 两台焊机通过特殊装置进行通讯, 保证两个电弧之间互不干扰, 并可使两根焊丝采用不同脉冲频率组合进行焊接, 通过多次试验研究发现, 通过一脉一滴的焊缝成形稳定, 飞溅低。这种焊接方法虽然电流大, 但焊接速度很快, 因此热输入量反而小, 焊接变形也很小。与其它的焊接技术相比熔敷速度快、焊接效率高、飞溅少。图 1 为双丝焊接系统组成示意图<sup>[1]</sup>。

焊接试板均采用双面 V 形 70° 坡口形式, 钝边为 5 mm, 间隙 2 mm, 每一面各焊三层。焊接参数见表 4。拉伸试样的加工为沿焊缝横向取样, 在 SHT4605 电液伺服万能试验机上进行拉伸试验; 在 HRB-150A 型洛氏硬度计上测量其洛氏硬度, 从焊

缝中心开始向母材逐点测量; 焊后各区微观组织的观察在 GX51 光学金相显微镜上进行, 在配有 INCA Energy—Oxford 能谱仪(EDS)的 Quanta 400—FEI 扫描电镜(SEM)上进行显微组织观察, 结合铝合金金相图谱对微区成分分析。在 AMRAY—1000B 扫描电镜上观察焊接接头拉伸断口形貌。

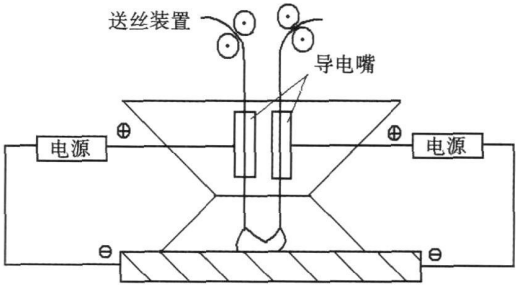


图 1 双丝焊系统组成示意图  
Fig. 1 Composition of twin wire welding

表 4 焊接工艺参数  
Table 4 Welding parameters

焊接方式	焊丝牌号	焊丝规格 Φ/mm	板材厚度 h/mm	焊接电流 I/A	电弧电压 U/V	焊接速度 v/(cm·min <sup>-1</sup> )	预热温度 T <sub>1</sub> /℃	层间温度 T <sub>2</sub> /℃	氩气流量 Q/L·min <sup>-1</sup>
单丝	5356	1.6	40	240~290	20~24	30	70~90	60~80	30
双丝	5356	1.6	40	170~220	21~24	35	70~90	60~80	45

2 试验结果及分析

2.1 7A52 铝合金单双丝焊接接头无损探伤

图 2 是 7A52 铝合金单双丝焊对接试板 X 射线探伤对比。由图 2a 可以看出, 单丝焊对接焊缝中可见大量气孔散布; 图 2b 表明双丝焊对接焊缝中只有少量 0.5~1 mm 气孔分布。这是由于采用双丝自动焊方法, 不仅焊接热输入减少, 降低了气孔倾向, 而且焊接过程中副丝对主丝的跟进延长了熔池凝固时间和熔池中气体析出时间, 也降低了产生气孔的倾向。

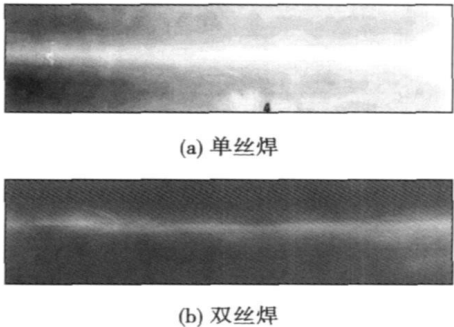


图 2 7A52 铝合金单双丝焊对接试板 X 射线探伤对比  
Fig. 2 X-ray photo of butt-welded plate of 7A52 aluminum alloy with single and double wire welding

2.2 单双丝焊后变形对比试验

对比采用单丝焊和双丝焊工艺焊接 40 mm 厚、角度为 35° 的单边 Y 形坡口对接焊缝, 单双丝焊接变形对比情况见图 3, 其中单丝焊焊后变形角度为

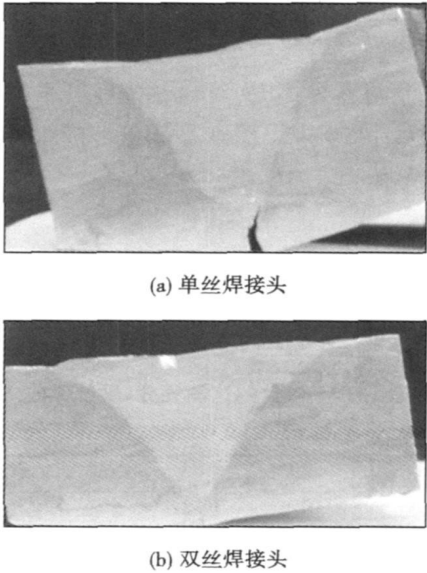


图 3 单双丝焊焊接变形对比  
Fig. 3 Comparison of weld distortion between single and double wire welding

24.6°(图 3a), 双丝焊焊后变形角度为 13.6°(图 3b)。从试验结果分析, 双丝焊由于焊接热量高度集中, 焊接热输入量小, 熔敷速度快, 焊接效率高, 焊后变形比单丝焊明显减小。

2.3 焊接接头的显微组织分析

7A52 铝合金单双丝焊焊缝显微组织分别如图 4a 和图 4b 所示, 由图可以看出焊缝组织均由  $\alpha(\text{Al}) + \beta(\text{MgZn}_2)$  相组成, 而且双丝焊焊缝组织较单丝焊焊缝组织更为致密, 晶粒细小, 这是由于双丝焊焊接速度快, 热输入量小的原因所致。

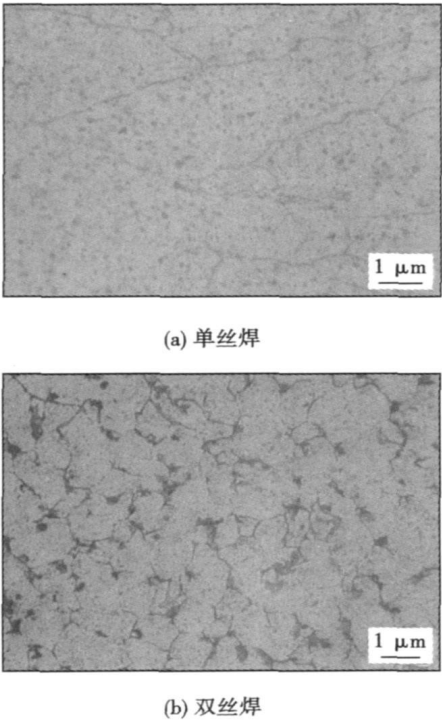


图 4 单双丝焊焊缝显微组织

Fig. 4 Microstructures of single and double wire welded metal

图 5 是单双丝焊焊缝能谱分析区。由于焊接时电弧温度很高(一般在 2 000 °C 以上), 而锌的沸点为 960 °C, 与焊接温度相比相差很大, 所以焊接时锌发生挥发烧损的现象。由于单丝焊焊接速度较慢, 焊接热输入量较大, 焊缝凝固时间相对较长, 使得 Zn 元素挥发时间加长; 从单双丝焊焊缝显微组织和能谱分析结果显示, 单丝焊焊缝选定区域(图 5a)中锌含量仅占焊缝组织的 0.94%, 而双丝焊焊缝选定区域(图 5b)中锌含量占焊缝组织的 1.81%, 由以上两个原因可以判定双丝焊焊缝中心锌含量相对较高, 由于 Zn 是强化相  $\text{MgZn}_2$  的主要元素, 所以锌的挥发损失是导致焊缝中心强度降低的原因之一。

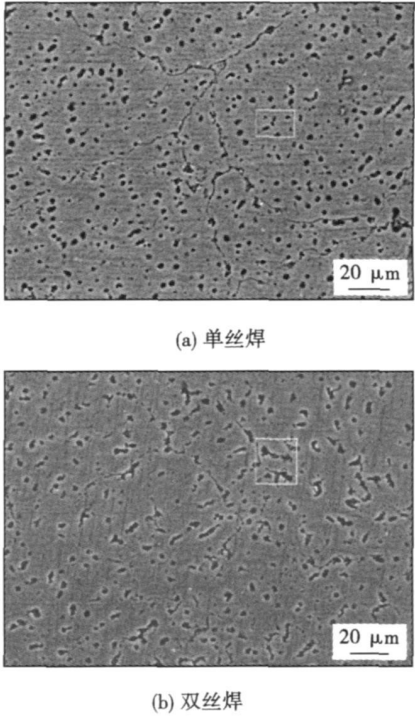


图 5 单双丝焊焊缝能谱分析区

Fig. 5 Analysis area of single and double wire weld

2.4 7A52 铝合金单双丝焊焊接接头硬度分布

在洛氏硬度计上从焊缝中心向母材侧逐点测试硬度, 测点间距为 5 mm。以焊缝中心为原点, 靠近母材一侧为正值的硬度曲线见图 6。由图可见, 双丝焊焊缝区硬度高于单丝焊焊缝, 这是由于双丝焊焊缝晶粒较单丝焊焊缝晶粒细小, 组织更为均匀的原因。从热影响区的硬度值比较发现, 双丝焊热影响区要比单丝焊热影响区窄, 且双丝焊热影响区的硬度高于单丝焊, 这是由于双丝焊热输入量相对较少, 焊缝散热速度快, 使得双丝焊热影响区的晶粒相对单丝焊要细小, 接头软化问题得到一定的控制。

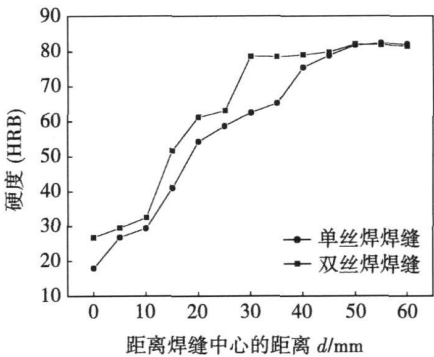


图 6 单双丝焊硬度对比曲线

Fig. 6 Graph contrast between single and double wire welding

2.5 单双丝焊接接头抗拉强度

表 5 为板厚 40 mm 7A52 铝合金单双丝焊接接头抗拉强度, 由表可见, 单双丝焊接接头抗拉强度分别为 250 和 269.2 MPa, 母材的抗拉强度为 410 MPa, 单双丝抗拉强度分别为母材的 60%, 66%。单双丝焊

接接头的断后伸长率分别为 5.8% 和 6.6%。说明铝合金采用双丝焊较单丝焊有较好的拉伸性能, 这与双丝焊焊后焊缝组织致密、晶粒细小有关。单双丝焊缝抗拉强度还与焊缝中心元素 Mg, Zn 含量有关, 它们在焊缝中形成主要的强化相 MgZn<sub>2</sub>。

表 5 单双丝 7A52 铝合金焊接接头的抗拉强度对比  
Table 5 Tensile strength contrast of the 7A52 welded joint between single and double wire welding

焊接类型	焊丝种类	抗拉强度 $R_m$ /MPa							备注
		1	2	3	4	5	6	均值	
单丝	5356	240	240	235	250	265	270	250	断于焊缝
双丝	5356	275	275	255	275	260	275	269.2	断于焊缝

2.6 单双丝焊接接头的拉伸断口扫描电镜分析

图 7 为 7A52 铝合金单双丝焊接接头拉伸断口形貌, 其中图 7a 为单丝焊接接头扫描断口形貌, 图 7b 为双丝焊扫描断口形貌。从图可以看出, 单双丝焊接接头的拉伸断口断面上分布着许多大小不同的韧

窝, 证明断口处发生了塑性流动, 且双丝焊断口韧窝较单丝焊韧窝要大而且深度也较深, 说明双丝焊焊接接头的抗拉伸性能较单丝焊要好。

3 结 论

(1) 通过对板厚为 40 mm 的 7A52 铝合金单双丝工艺对比研究发现, 双丝焊接头较单丝焊接头综合性能更为优良。

(2) 双丝焊焊接接头可以减少锌的挥发, 提高焊缝强度。

参考文献:

[ 1 ] 高云喜, 孙学斌. 双丝自动焊接技术应用研究[ J ]. 兵器材料科学与工程, 2006, (9): 91—93.  
[ 2 ] 余 进, 王克鸿, 徐越兰, 等. 7A52 铝合金双丝焊接头的组织与性能[ J ]. 焊接学报, 2005, 26(10): 87—89.  
[ 3 ] 明 珠, 马新沛, 王克鸿, 等. 厚板铝合金双丝气体保护焊工艺[ J ]. 焊接, 2004, (10): 25—28.  
[ 4 ] Janaki R G, Mitra T K, Shankar V. Microstructural refinement through inoculation of type 7020 Al-Zn-Mg alloy welds and its effect on hot cracking and tensile property[ J ]. Material Process Technology , 2003, 42: 174—181.

作者简介: 张传臣, 男, 1981 年出生, 硕士研究生。主要从事铝合金焊接方向的研究。已发表论文 2 篇。

Email: zhangchuanchen@qq.com

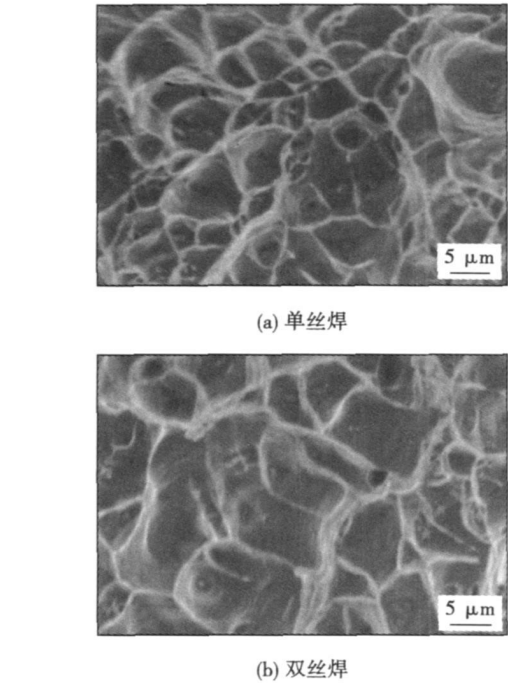


图 7 单双丝焊接接头断口扫描电镜形貌  
Fig. 7 SEM micrographs of tensile fracture between single and double wire welded joints

Cu-Al<sub>2</sub>O<sub>3</sub> gradient coatings have not distinct componential saltation and macroscopic interface, and the coatings show the characteristic that structure is not uniform macroscopically but consecutive microscopically. The abrasability of the coatings is best when the content of Al<sub>2</sub>O<sub>3</sub> is 80% and the abrasability is three times than the substrate. The abrasability of pure ceramic coatings decreases as the Al<sub>2</sub>O<sub>3</sub> content increases. The wear mode changed from cutting and ploughing to the hard phase breaking and pull-out.

**Key words:** plasma spray; Al<sub>2</sub>O<sub>3</sub> ceramic; gradient coatings; wear

**Analysis of strengthening mechanism of ultrasonic impact treatment of 2A12 aluminum alloy weld joint** LI Zhanming<sup>1</sup>, ZHU Youli<sup>1</sup>, WANG Kan<sup>2</sup>, Wang Yong<sup>1</sup> (1. Faculty of the Remanufacturing Engineering, Academy of Armored Force Engineering, Beijing 100072, China; 2. Department of Scientific Research, Academy of Armored Force Engineering, Beijing 100072, China). p55—58

**Abstract:** Aluminum alloy 2A12 welded joint was strengthened by ultrasonic impact treatment (UIT). The microstructure of welded joint with and without UIT was studied by optical microscope. Surface micro-hardness distribution across the weld joint and that along the depth direction of the cross section of the weld bead were measured by a micro-hardness tester. Residual stress distribution along the transverse direction of the weld joint surface was investigated by X-ray diffraction techniques. The micro-structural strengthening mechanisms via UIT were investigated. Results show that metallurgical structure of the near surface material of the weld zone was densified due to ultrasonic impact treatment. The depth of plastic deformation manifested by the textured structure extended up to about 300 μm from the surface. Defects such as gas cavity and shrinkage porosity in the weld zone were reduced substantially after ultrasonic impact treatment. The hardness values of the weld zone and the surface of the welded joint were improved distinctly. High tensile weld residual stress was eliminated and compressive residual stress was induced by UIT.

**Key words:** ultrasonic impact treatment; aluminum alloy; microstructure; micro hardness; residual stress

**Effect of germanium on shearing strength and fracture surface of SnAgCu/Cu soldering joint** MENG Gongge<sup>1</sup>, LI Caifu<sup>2</sup>, YANG Tuoyu<sup>3</sup>, CHEN Leida<sup>1</sup> (1. School of Material Science & Engineering, Harbin University of Science and Technology, Harbin 150040, China; 2. Institute of Metal Research Chinese Academy of Sciences, Shenyang 110016, China; 3. Anhui Science and Technology University, Bengbu 233100, Anhui, China). p59—62

**Abstract:** In Periodic Table of the Elements, germanium (Ge) is adjacent to tin. They are both the elements in the main group IV and resemble each other in physical and chemical property. A little element Ge was added into lead-free solder Sn2.5Ag0.7Cu (0.25, 0.5, 0.75, 1.0 wt%), and the shear test specimens were designed and welded. The joint shearing strengths were measured and fracture surfaces were analyzed by scanning electron microscope and energy dispersive X-ray analysis method. The result indicates that the shearing strength of the joint increases obviously. The joint fracture forms of the Sn-Ag-Cu-Ge lead-free solder are

mainly ductile fracture, and most of them have secondary cracks. Lots of dimples formed on the fracture surface when adding element Ge, and IMC Cu<sub>6</sub>Sn<sub>5</sub> play a part on the dimple forming.

**Key words:** lead-free solder; shearing strength; fracture surface; germanium

**Digital control system based on DSP for pulsed MIG welding**

PENG Haiyan<sup>1,2</sup>, HUANG Shisheng<sup>1</sup>, WU Kaiyuan<sup>2</sup>, WANG Zhermin<sup>1</sup> (1. Guangdong Polytechnic Normal University, Guangzhou 510635, China; 2. South China University of Technology, Guangzhou 510640, China). p63—66

**Abstract** A digital control system with TMS320LF2407A DSP as its kernel was designed aiming at some deficiencies in the simulating control system and single-chip control system, such as poor flexibility, control precision and reliability. The hardware circuit and software flow chart were presented. In this control system, fuzzy control and close-loop control were applied to control the arc length, and modification mechanism of PFM to modify the pulse shape. The experimental results show that the pulse MIG welding digital control system based on DSP has the advantages of quicker response, better reliability, more stable arc length and better-formed welding seam, over the traditional simulating control system and single-chip control system; furthermore, by using the fuzzy control theory, the stability of welding process is improved and the optimization of multi-parameters match is solved.

**Key words:** DSP; pulse MIG welding; digital control; fuzzy control

**Analysis on single and double wire welding technology of 7A52 aluminum alloy** ZHANG Chuanchen<sup>1</sup>, CHEN Fulong<sup>1</sup>, GAO Yunxi<sup>2</sup> (1. College of Materials Science and Engineering, Inner Mongolia University of Technology, Hohhot 010051, China; 2. Baotou North Engineering Development Co. Ltd, Baotou 014033, Inner Mongolia, China). p67—70

**Abstract** The thick plate of 7A52 aluminum alloys were welded by single and double wire gas shielded arc welding with ER5356 filler. The distortion of the welded joints is analyzed. The microstructure, hardness and tensile strength of single and double wire welded joints are studied. The comparison between single and double wire welding show that the distortion of the double wire welded joint is smaller, the microstructure of double wire welded metal is tighter than the single one, the heat-affected zone is narrower, and the hardness is higher. The tensile strength increase by 7.7% compared to single wire welding. Energy spectrum analysis shows that the volatilization of Zn could be restrained by using double wire welding.

**Key words:** 7A52 aluminum alloy; single wire welding; double wire welding; microstructure; mechanical property

**Welding process of magnetically induced rotating MAG** LIU Zhongbao<sup>1</sup>, HUA Aibing<sup>2</sup>, YIN Shuyan<sup>2</sup>, CHEN Shujun<sup>2</sup>, ZHANG Xiaoliang<sup>2</sup> (1. Guangdong Electric Power Design Institute, Guangzhou 510600, China; 2. College of Mechanical Engineering and Applied Electronics Technology, Beijing University of Technology, Beijing 100022, China). p71—74